Energy Method for Approximating Overland Tsunami Flows

David L. Kriebel, Ph.D., P.E., M.ACSE[1]; Patrick J. Lynett, Ph.D., M.ASCE[2]; Daniel T. Cox, Ph.D., P.E., M.ASCE[3]; Catherine M. Petroff, Ph.D., P.E., M.ASCE[4]; Ian N. Robertson, Ph.D., S.E., M.ASCE[5]; and Gary Y. K. Chock, S.E., M.ASCE[6]

Abstract: This paper applies a simple energy method to predict characteristics of overland tsunami flows based on extrapolation of the energy grade line between the shoreline and the tsunami run-up limit. Starting with a mapped run-up or inundation limit from tsunami hazard maps or from field surveys, the method reconstructs maximum inundation depths and velocities across a flooded topographic transect to the shoreline. The energy method is evaluated first in comparison with thousands of numerical simulations conducted on idealized topographies using a free-surface wave model. The method is then evaluated in more detailed simulations over realistic topography using a second tsunami-evolution model. Finally, the method is evaluated against field observations of inundation depths from tsunami events in Chile and Japan. In all cases, inundation depths are predicted quite well, with little bias across a wide range of flow conditions and topographic conditions. Predicted velocities show less precision but seem to predict the general velocity decay from shoreline to run-up limit. The method then overestimates and provides a conservative estimate of the maximum momentum flux. **DOI: 10.1061/(ASCE)WW.1943-5460.0000393.** *© 2017 American Society of Civil Engineers.*

Downloaded from ascelibrary.org by Southern California University on 05/19/17. Copyright ASCE. For personal use only; all rights reserved.

Introduction

This paper presents a simplified energy method (EM) for estimating overland tsunami flow characteristics based on analysis of the energy grade line between the shoreline and the tsunami run-up or inundation limit. This method assumes that at least one key tsunami inundation characteristic is known, either the inundation depth at the shoreline or the inland inundation limit of tsunami run-up. The proposed method then allows an approximate reconstruction of the maximum flow depth and maximum velocity for locations across the inundation zone.

The basic idea behind the method is that in many applications, certain features of the hydraulic energy of an overland tsunami flow are known or can be specified at either the shoreline boundary or at the run-up limit. Overland tsunami flows on the open coast are often approximately unidirectional for timescales on the order of minutes, and in comparison with wind waves, the flows are slowly varying in time after the passage of the bore or surge front. As a result, the hydraulic energy of the flow can be approximated as a quasi-steady sum of the potential and kinetic flow energy, as measured by the flow depth and velocity head. At the shoreline, where ground elevation is zero, the energy grade line is located at a height above the water surface equal to the velocity head. At the run-up limit, the hydraulic energy is zero, and the energy grade line intersects the ground topography. In between the shoreline and the run-up limit, the slope of the energy grade line can be established using appropriate expressions for energy losses attributable to bottom friction, wave breaking, and the turbulence of the advancing flow.

The EM can be applied if at least one water level is known across a topographic transect. If the tsunami height at the shoreline is known, then the method can be used to track the advancing energy across the flooded topographic transect to predict the run-up limit. If the tsunami run-up limit is known, from inundation maps showing the tsunami hazard zone or from field surveys following tsunami events, then the method can be used to back-calculate the flow depths and velocities across the transect to the shoreline. In both cases, the method allows an estimate of maximum flow depth and velocity for locations across the flooded transect between the shoreline and the run-up limit. If an inundation level is known at any location across the transect, from a field survey, for example, then the method can be used to roughly reconstruct elevations and velocities on either side of that point, with improved results if additional inundation levels are known and used as constraints.

Background

Despite the availability of high-fidelity numerical models for predicting tsunami flows, there is still a need for simplified methods of predicting tsunami inundation depths and flow velocities for use in engineering practice. The proposed method was developed for inclusion in building codes and standards for use in designing the structural integrity of certain critical building facilities to resist tsunami flows. In a design code application, structural engineers would need a conservative estimate of tsunami inundation depth and flow velocity at a structure site for use in load calculations. Similar applications might include highway engineers involved in checking the adequacy of coastal highways and bridges, geotechnical engineers involved in checking scour potential from tsunami flows, or

[1]Professor, U.S. Naval Academy, Annapolis, MD 21402 (corresponding author). E-mail: kriebel@usna.edu

[2]Professor, Univ. of Southern California, Los Angeles, CA 90089. E-mail: plynett@usc.edu

[3]Professor, Oregon State Univ., Corvallis, OR 97331. E-mail: dan.cox@oregonstate.edu

[4]Affiliate Professor, Univ. of Washington, Seattle, WA 98195. E-mail: cpetroff@uw.edu

[5]Professor, Univ. of Hawaii at Manoa, Honolulu, HI 96822. E-mail: ianrob@hawaii.edu

[6]President, Martin & Chock, Inc., 1132 Bishop St., Suite 1550, Honolulu, HI 96813. E-mail: gchock@martinchock.com

Note. This manuscript was submitted on November 16, 2015; approved on December 21, 2016; published online on April 27, 2017. Discussion period open until September 27, 2017; separate discussions must be submitted for individual papers. This paper is part of the ***Journal of Waterway, Port, Coastal, and Ocean Engineering***, © ASCE, ISSN 0733-950X.

municipal engineers checking the potential tsunami impact on other infrastructure in the community. In each of these cases, the end-user would be a practicing civil engineer but probably not a tsunami expert with any experience in running detailed numerical models.

Several simplified methods now exist in the tsunami literature to predict certain tsunami characteristics. One approach includes empirical equations for tsunami run-up [e.g., Li and Raichlen (2003) or Fuhrman and Madsen (2008)]. These were generally developed from small-scale laboratory data and by necessity use idealized bathymetry and topography, typically a flat-bottom offshore with a uniform linear slope extending onshore, along with solitary wave conditions that can be generated in a wave tank. The predicted flow property is the vertical run-up distance, and these methods do not include predictions of any other flow properties across the topographic transect.

A second simplified approach includes analytical solutions of shallow-water wave equations for tsunami interaction with a plane slope [e.g., Shen and Meyer (1963), Synolakis (1987), Madsen and Schäffer (2010), or Yeh (2006)]. Advantages of this approach are the use of nonlinear governing equations that can model the time-dependent uprush and downrush to develop estimates of flow depth, flow velocity, and properties related to forces on structures, such as the momentum flux [e.g., FEMA (2012)]. However, analytical models have numerous limitations for application to realistic field conditions because they require a uniform plane slope; use of sinusoidal, solitary, or N-waves as input; and the assumption of a smooth slope with no roughness.

A third simplified approach involves the application of dam-break equations [e.g., Chanson (2006)]. In this approach, the tsunami wave at the shoreline is approximated by a dam break, and a nonlinear shallow-water equation (St. Venant equation) is used to predict not only the run-up limit but also the time-dependent flow depth and flow velocity across the inundation zone. The limitations of this approach are, again, the need for uniform profile slopes and uniform roughness coefficients because the method assumes a linear beach slope with a single overall roughness to make the nonlinear shallow-water equations tractable.

The proposed EM seeks to overcome some of the limitations of the empirical, analytical, and dam-break methods for practical application. The primary advantage of the energy-grade-line approach is that it can be used for irregular topography and is not limited to uniform plane slopes. Ground slopes can be specified in piecewise linear segments, and both positive and negative local ground slopes can be used. A second advantage is that spatially varying ground roughness can be included. The method models head loss using the Manning equation, which relies on ground roughness as expressed in terms of the Manning n parameter. This can vary in a piecewise manner across the topographic transect from open beach conditions near the shoreline to wooded or urban topography inland. A third advantage is that the method does not rely on any specific tsunami waveform and is not limited to solitary wave profiles.

The EM, as discussed in this paper, relies on a known run-up limit from tsunami inundation maps as input. These inundation maps, produced by national, state, or local agencies (NOAA's National Tsunami Hazard Mitigation Program website has numerous examples), are usually produced from sophisticated numerical simulations starting with ground motions at a generating source and thus are not dependent on any idealized waveform. Although detailed simulations were performed to generate the tsunami inundation (or hazard) maps, additional information is not usually displayed on the maps or archived for convenient use by end-users. For example, although the numerical codes certainly include detailed prediction of overland flow velocities and depths at any numerical grid point, this information is not generally displayed on maps and is usually not available to end-users who did not run the model or generate the map. All that a typical end-user would have available would be the modeled run-up limit (i.e., inundation distance and vertical elevation).

The concept of applying an energy grade line to overland flows between the shoreline and the run-up limit is not new. FEMA guidance for wind-wave run-up on composite slopes adopts a similar approach (FEMA 2007), developed by French (1982) for the Casco Bay, Maine, flood insurance study. The FEMA approach is similar to that proposed here but was applied with different input conditions. The FEMA method first estimates a hypothetical run-up on the steep beach-face slope near the shoreline as if the slope extends indefinitely landward. For cases where the hypothetical run-up elevation exceeds the actual beach berm elevation, the energy approach is used to account for berm overtopping and flow landward from the beach berm. A similar approach was later proposed by Cox and Machemehl (1986) for short wave attenuation. Whereas the FEMA method uses Manning's n value to reflect energy losses, the Cox and Machemehl approach uses a breaking-wave dissipation term, not ground roughness.

Both the FEMA method and the Cox and Machemehl method were applied to short-period wind waves. It may be expected that the application of a similar energy method to tsunami flows may produce better results than the application to wind waves. Overland tsunami flows occur over a longer time period and over longer spatial dimensions, and they may act as quasi-steady near-uniform flows at any one location across the tsunami inundation zone. A limitation of the EM, however, is that it assumes that the maximum inundation depth and maximum velocity occur at the same time. For cases in which the tsunami propagates inland over mild slopes without significant reflection, this approximation may be reasonable. But in other cases with steeper slopes, wave reflection leads to conditions where maximum depth and maximum velocity are poorly correlated.

Application in ASCE7 Standard for Tsunami Loads and Effects

The proposed EM was developed as a simplified analysis of overland tsunami flows for inclusion in a new ASCE standard for tsunami-resistant buildings and other structures to be contained in a future edition of the ASCE Standard 7, "Minimum design loads on buildings and other structures" (ASCE 2013). In January 2011, ASCE formed a Tsunami Loads and Effects Committee to develop guidelines for including tsunami loads on buildings for the first time in an upcoming revision of ASCE 7. This new standard will apply to major new buildings constructed in tsunami hazard zones to promote life-safety of critical structures such as schools, hospitals, police/fire stations, major hotels, and other buildings with occupancy greater than 300 people. The standard would not apply to most residential structures.

As with other ASCE 7 provisions, standards for tsunami loads will be written with a simplified prescriptive method included in the standard. This is intended to be generally conservative and something an end-user can adopt without additional analysis. But the provisions will also allow a user to apply more detailed methods, including detailed numerical models or physical model studies, to refine the load calculations. This allows the user to invest in more detailed site-specific analysis and possibly obtain less conservative results.

For tsunamis, ASCE 7 will reference tsunami hazard maps that will indicate an inland inundation distance and corresponding tsunami run-up elevation based on a 2,500-year recurrence interval

Downloaded from ascelibrary.org by Southern California University on 05/19/17. Copyright ASCE. For personal use only; all rights reserved.

maximum-considered tsunami event, an event consistent with earthquake design standards and having a 2% probability of being exceeded in a 50-year project lifetime. The intent is to use the maps to define a tsunami hazard zone that extends from the shoreline to the inundation limit, and then to require load calculations for hydrostatic, hydrodynamic, and debris loads for any major structure located within this zone. The tsunami hazard maps will be based on sophisticated probabilistic modeling of tsunami sources, with tsunami propagation and overland inundation performed by state/federal agencies using approved/certified tsunami wave-propagation models.

The ASCE 7 tsunami hazard maps will indicate the inland extent of run-up and inundation. But because of limitations on the amount of information that can be contained in the ASCE 7 standard, hazard maps would not directly indicate tsunami wave heights, inundation depths, or flow velocities at other locations between the offshore and the mapped run-up limit. It is noted that hazard maps showing more detail of the cross-shore variation in inundation and velocity have been produced [e.g., Taubenböck et al. (2013)], but these have focused on small geographic areas and generally cannot be produced efficiently for use in a national mapping program of the kind required for the ASCE 7 standard. For the ASCE 7 standard, one of the key parts of the tsunami loading provisions is then to prescribe a method that would allow a user to estimate design flow depths and velocities, knowing only the overland topography and the mapped run-up/inland inundation limit.

The proposed EM was therefore developed as a simple method of providing a reasonable and realistic, yet generally conservative estimate of flow characteristics across the tsunami inundation zone. Because the final inland extent of tsunami inundation is known from the hazard maps, and because the vertical run-up elevation of this limit is known from ground topography, the final potential energy of the tsunami flow is known a priori. Use of traditional energy-grade-line methods then allows the tsunami energy to be traced back out to the shoreline, accounting for both elevation and topographic changes and the energy losses that occur between the shoreline and the run-up or inundation limit.

Energy Method

The EM is based on the premise that a hydraulic energy budget can be established to account for flow energy and energy dissipation between the shoreline and the inundation or run-up limit for tsunami flows. General characteristics of the energy grade line between the shoreline and run-up limit are depicted in Fig. 1.

At the shoreline, where the pretsunami water depth, d, is zero, the tsunami flow energy may be defined as the sum of potential and kinetic energy. The potential energy is proportional to the wave or bore height over ground, h_o, and the kinetic energy can be represented by the velocity head, $U_o^2/2g$, where U_o is the depth-averaged flow speed at the shoreline. Therefore, the total energy grade line at the shoreline has an elevation equal to the incident velocity head $E_o = h_o + U_o^2/2g$. This establishes an upper bound on the maximum energy level across the topography because the energy grade line then decreases between the shoreline and the run-up limit.

At the inland extent of the run-up, the kinetic energy of the flow has been reduced to zero, and the potential energy is expressed in the vertical run-up elevation, R, so that the height of the energy grade line at the run-up limit is $E_R = R$. One interesting feature of the run-up limit is that the vertical elevation, R, may be higher or lower than the tsunami wave height at the shoreline, h_o. The run-up elevation, R, is generally higher than h_o for steep-slope transects and lower than h_o for mild-slope transects. But R is always below the incident energy grade line at the shoreline, E_o, because of the energy losses that occur as a result of flow friction, breaking, and turbulent energy dissipation between the shoreline and the run-up limit.

At any point in between the bounding limits, the specific energy above the ground surface is given by

$$E = h + \frac{U^2}{2g} \tag{1}$$

where h and U = local depth and velocity, respectively. The local energy grade line, or total energy, can be related to this specific energy by including the ground elevation, z, or by accounting for head losses, H_L, from the shoreline to the point of interest as

$$E + z = E_o - H_L \tag{2}$$

If a transect is discretized into finite horizontal sublengths, Δx, and if the incremental head loss per unit length or friction slope, S, is defined in each sublength, then the total head loss can be given by the accumulated losses across the flooded transect as

$$H_L = \sum S\,\Delta x \tag{3}$$

The gradient in energy across the transect is then given by

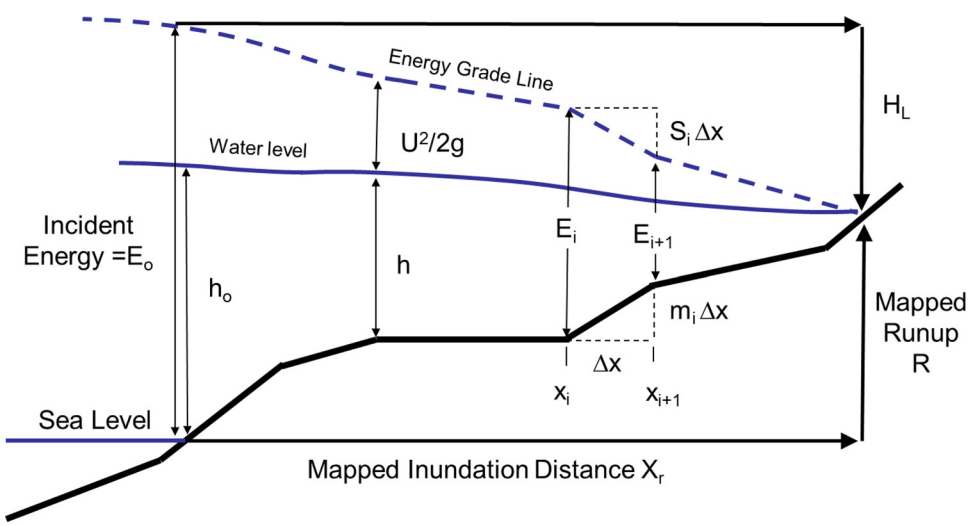

Fig. 1. Illustration of energy method across inundated transect; incident tsunami flow is from left to right

J. Waterway, Port, Coastal, Ocean Eng., 2017, 143(5): -1--1

Downloaded from ascelibrary.org by Southern California University on 05/19/17. Copyright ASCE. For personal use only; all rights reserved.

$$\frac{dE}{dx} = -(m + S) \tag{4}$$

where $m = dz/dx$ is the local ground slope; and $S = dH_L/dx$ is the local friction slope.

Because Eq. (4) for the energy gradient dE/dx is a first-order differential equation, this can be solved numerically with a number of different numerical schemes as long as a boundary value for energy is known. This can be done with a known energy at the shoreline E_o, if the flow depth and velocity are known, using a forward solution and stepping inland to predict the run-up limit. This can also be done if the run-up limit, energy level E_R, is known from inundation maps or field surveys, in effect starting at the landward run-up limit and stepping back out to sea to the shoreline. Alternatively, one can implement an iterative procedure to select conditions at the shoreline, step to the run-up limit, and compare to the known run-up limit, with subsequent adjustments to shoreline values until the run-up limit is matched. In practice, the method seems robust enough that many different numerical solution schemes can be used to give essentially the same results.

One simple, explicit form of a numerical solution of Eq. (4) can relate the hydraulic energy between any two points across the transect as

$$E_{i+1} = E_i - (m_i + S_i)\ \Delta x_i \tag{5}$$

This can be expressed in terms of basic variables of inundation depth and flow velocity as

$$\left(z + h + \frac{U^2}{2g}\right)_{i+1} = \left(z + h + \frac{U^2}{2g}\right)_i - S_i\ \Delta x_i \tag{6}$$

The slope of the energy grade line, S, can be represented through use of the Manning equation, in this case using values from Point i as

$$S_i = \frac{U_i^2}{(k/n_i)^2\, h_i^{4/3}} \tag{7}$$

where k = s a conversion factor (k = 1 for SI units, k = 1.49 for Imperial units); and n_i = Manning coefficient, which can be defined for the local computational grid point to reflect ground roughness effects on frictional and turbulent energy losses. It is noted that Manning's n does not normally represent energy dissipation attributable to wave breaking, but here it is used as a single coefficient to reflect the total energy loss from all physical sources of energy dissipation.

Substituting Eq. (7) into Eq. (6) yields

$$\left(z + h + \frac{U^2}{2g}\right)_{i+1} = \left(z + h + \frac{U^2}{2g}\right)_i - \left[\frac{U^2\,\Delta x}{(k/n)^2\, h^{4/3}}\right]_i \tag{8}$$

A complication with the EM in Eq. (8) is that there are two unknowns: inundation depth h and flow velocity U. As a result, a second relationship between h and U is required. The approach used here is to adopt the Froude number as a basic relationship for shallow-water flows in the form

$$U = \mathsf{F}\,(gh)^{1/2} \tag{9}$$

where F can be treated as a coefficient and modified according to flow conditions. Numerous values of F have been suggested in the literature. For surge over dry land with no friction, it is known from theoretical solutions using the method of characteristics that the leading edge of the surge theoretically has a supercritical Froude number of 2 [e.g., Chanson (2006)], whereas flows behind the leading tip have lower Froude numbers. In the energy-grade-line approach of FEMA (2007), as developed by French (1982), it was argued that if contributions from potential and kinetic energy are equal, then $\mathsf{F} = \sqrt{2}$ should apply. Although these values may apply at the leading edge, lower values of F are typically more appropriate behind the leading edge.

Introducing Eq. (9) into Eq. (8) then yields an expression for inundation depth h as

$$\left(z + h + \frac{1}{2}\,\mathsf{F}^2\, h\right)_{i+1} = \left(z + h + \frac{1}{2}\,\mathsf{F}^2\, h\right)_i - \left[\frac{g\,\mathsf{F}^2\,\Delta x}{(k/n)^2\, h^{1/3}}\right]_i \tag{10}$$

In early trials of the energy method in Eq. (10), the Froude number was adopted as a true constant across the topographic transect. Subsequent trials comparing Eq. (10) to results of numerical wave models indicated that better results were achieved by varying the Froude number across the transect, starting with the highest value at the shoreline and diminishing to a Froude number of zero at the run-up limit.

The Froude-number decay across a topographic transect does not have a firm theoretical basis. Some guidance was obtained from both Shen and Meyer (1963) and Yeh (2006), who showed that the maximum flow speed of a tsunami bore has a decay in the landward direction proportional to the square root of the distance between the shoreline and the run-up or inundation limit. As will be discussed in a subsequent section of this paper, comparisons of the EM and nonlinear computer models based on nonlinear shallow-water wave equations helped resolve the issue, with the best results obtained when using an empirical Froude-number decay in the form of

$$\mathsf{F} = \mathsf{F}_o\left(1 - \frac{x}{x_R}\right)^{1/2} \tag{11}$$

where the value of F_o = 1 applies at the shoreline where x = 0, and where the effective local Froude number then decays toward the run-up limit at distance X_R from the shoreline. This was investigated by Weibe (2013), who found that either a linear decay or a square-root decay provided improved results compared with simply using a constant value of F, but the square-root decay seemed to be preferable. Results are also not too sensitive to the choice of Froude number at the shoreline. As will be discussed, F_o between 0.85 and 1.0 provided nearly identical results, with F_o = 1.0 being adopted as the most intuitive result for application. Fritz et al. (2012) show from field surveys that an incident Froude number of approximately 1.0 is reasonable but that the outflow may have a larger Froude number. Subsequent work by Carden et al. (2015) shows that for bore conditions, the Froude number at the shoreline should be 1.3 instead of 1.0.The EM solution in Eqs. (10) and (11) can be applied in two ways.

The most straightforward way would be to start at the shoreline with a known inundation depth h_o, then step forward (inland) to the run-up limit. Eqs. (10) and (11) adopt this approach. In practice, however, the tsunami inundation depth at the shoreline is not normally known and is not normally included on tsunami hazard maps. Instead, the inundation limit or run-up limit is usually known from tsunami hazard maps. In this application, the end result for run-up is known, and Eqs. (10) and (11) are used to step backward across the topographic transect from the known run-up location to the

J. Waterway, Port, Coastal, Ocean Eng., 2017, 143(5): -1--1

Downloaded from ascelibrary.org by Southern California University on 05/19/17. Copyright ASCE. For personal use only; all rights reserved.

shoreline. In this case, the explicit formulation of head loss is evaluated at the landward grid point so that a revised version of Eq. (10) is obtained as

$$\left(z+h+\frac{1}{2}\ \mathsf{F}^2 h\right)_i = \left(z+h+\frac{1}{2}\ \mathsf{F}^2 h\right)_{i+1} + \left[\frac{g\ \mathsf{F}^2\ \Delta x}{(k/n)^2\ h^{1/3}}\right]_{i+1} \tag{12}$$

Monte Carlo Optimization with *COULWAVE*

The EM was evaluated using extensive comparisons with the Boussinesq wave model *COULWAVE* (Lynett et al. 2002). The general approach was to perform several thousand Monte Carlo simulations using *COULWAVE* as a benchmark, then compare the inundation properties of the Boussinesq model output with that of the EM. The primary objectives of this work were to determine the optimal choice for the free parameter controlling the Froude number at the shoreline, F_o, and to assess the ability of the EM to provide a physical result for a wide range of possible onshore topographic profiles and wave conditions.

The Monte Carlo simulation with *COULWAVE* used 36,000 random combinations of topographic transects and incident tsunami wave conditions. Piecewise linear bathymetric and topographic profiles were selected using random combinations of slope between fixed points across the transect. The offshore profile, connecting depths of 100 to 0 m, was constructed with a single linear segment with a slope chosen randomly between 1/10 and 1/500 and a mean of approximately 1/60. Onshore, the initial dry beach profile was composed of 20 individual linear segments with randomly chosen slope and length. The beach slope parameters chosen for the Monte Carlo analysis were selected to cover a range of realistic beach profiles. Uniformly distributed random numbers were used to select slopes for each segment that varied between 0.06 and –0.04, with a mean of 0.01 (1/100). This slope formulation allows for both positive and negative slopes, in addition to flat slopes, and will be biased toward positive mild slopes. The length of each of the 20 individual onshore segments was selected from 0 to 300 m. Finally, the onshore elevation was not permitted to dip below the shoreline elevation or to exceed a 50-m elevation. In this analysis, 800 unique beach transects were selected that were judged to be representative of many natural beaches.

The incident wave conditions were constructed as a waveform pulse representing idealized tsunami waveforms made of a single crest and a single trough, which can reverse positions so that waveforms with leading positive elevation or leading depression can be included. Although this is a simplification of a real tsunami, the waveform captures the essential nature of a tsunami as an N-wave as discussed by Tadepalli and Synolakis (1996), and the configuration of the N-wave has a leading-order impact on the overland flow characteristics of a tsunami, according to Carrier et al. (2003). The amplitudes of the two pulses were selected as 0 to 15 m in increments of 2.5 m, producing trough-to-crest heights that varied from 2.5 to 15 m. The wave period, defined as the time from the start of the first pulse to the end of the second, was selected as 600, 1,200, or 2,400 seconds. In total, 45 combinations of amplitudes and period were included. Coupling of the 45 wave conditions with the 800 transect combinations resulted in 36,000 unique simulations.

The incident waveform was forced through the offshore boundary of the Boussinesq-type simulation at the 100-m offshore depth and was then simulated over time until the maximum run-up occurred. A Manning's n friction factor of 0.025 was used at all grid points. Results were then saved every 10 m across the initially dry transect, with saved output consisting of the maximum flow depth, flow speed, and momentum flux at each grid point and the maximum run-up location. Using the Boussinesq-predicted run-up point and the onshore topographical profile, the EM was then used to predict the maximum flow depth, flow speed, and momentum flux across the entire profile, using the same Manning's n of 0.025.

It is not reasonable to present the individual transect comparisons for the very large number of simulations performed. An attempt to present information from all 36,000 simulations simultaneously is provided in Fig. 2. This figure shows all of the point-to-point flow depth comparisons (Boussinesq to EM) across the entire length of each flooded onshore transect. On average, each transect contained roughly 20 flooded grid points, and thus Fig. 2 in fact shows over 700,000 individual point-to-point flow depth comparisons. In Fig. 2, the EM method uses an initial Froude number of 1.0 with the square-root decay from Eq. (14). In addition to the point cloud, the mean regression line between the data and the standard deviation bounds are shown. Because the mean regression line lies above the 1:1 (45°, straight line), this implies that, in the mean sense, the EM yielded a lesser flow depth than the Boussinesq simulation. However, this bias was somewhat weak, falling just within a single standard deviation.

The standard deviation for the maximum flow speed, conversely, was not small. Fig. 3 shows the point-to-point comparisons of speed. Here, the EM evidenced a mean underprediction bias for flow speeds less than 4.5 m/s and an overprediction bias for flow speeds greater than 4.5 m/s. This bias was small in the mean sense across all flow speeds, but the standard deviation of the EM speed predictions was approximately 2 m/s for all flow speeds. Therefore, at low flood speeds, the EM was found to be very imprecise, and this lack of precision decreased linearly with flow speed. Confidence in the EM velocity prediction is then better at higher flow velocities. In sensitivity studies, it was found that velocities were predicted best, and with little bias, for positive ground slopes but that there was a general underprediction bias for negative ground slopes. The primary

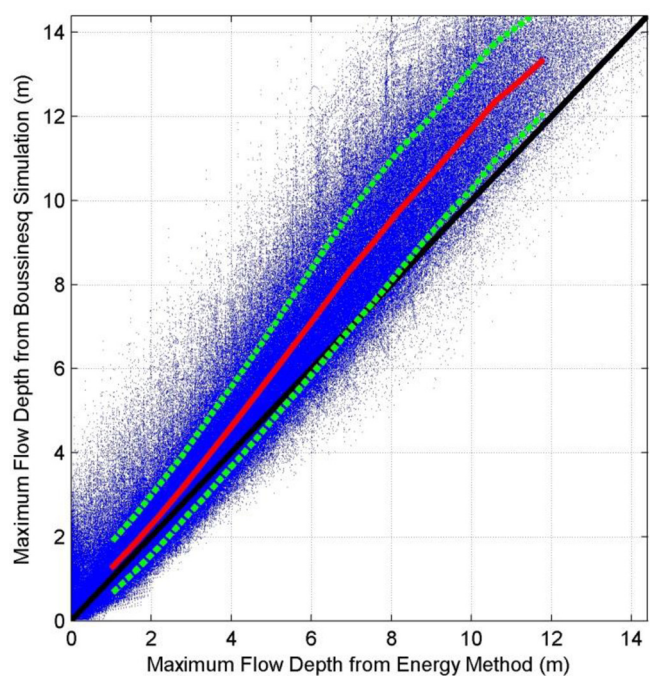

Fig. 2. Flow-depth comparison between Boussinesq and EM results; the dots are the individual point-to-point comparisons, the solid curve is the mean regression line of the point cloud, and the dashed curves are the standard deviation bound from the mean

J. Waterway, Port, Coastal, Ocean Eng., 2017, 143(5): -1--1

Downloaded from ascelibrary.org by Southern California University on 05/19/17. Copyright ASCE. For personal use only; all rights reserved.

Downloaded from ascelibrary.org by Southern California University on 05/19/17. Copyright ASCE. For personal use only; all rights reserved.

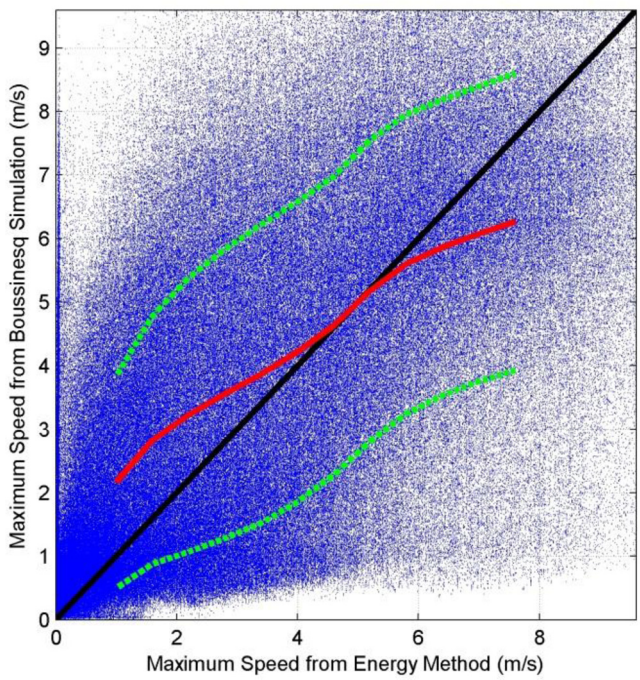

Fig. 3. Flow-speed comparison between Boussinesq and EM results

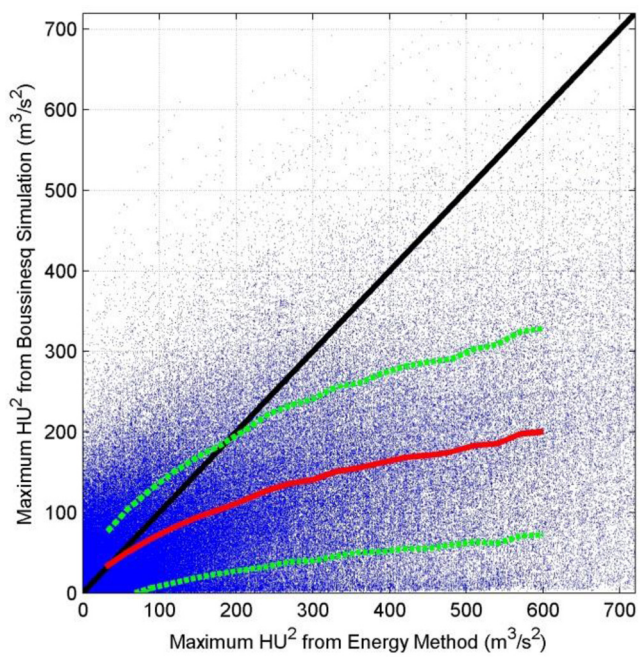

Fig. 4. Momentum-flux comparison between Boussinesq and EM results

reason for this is that the EM does not account for rapidly varying flow conditions that may occur over the negative ground slopes.

For the last type of data evaluation, Fig. 4 shows the point-to-point comparisons for maximum momentum flux, computed as $M = h\,U^2$. From the mean regression line, it is evident that the EM overpredicted maximum momentum flux for all predicted values greater than 25 m^3/s^2. This overprediction bias is driven by the observation that in the Boussinesq simulations, the maximum momentum flux rarely occurred at the time of both maximum flow depth and maximum flow speed; in the EM method, the two were always

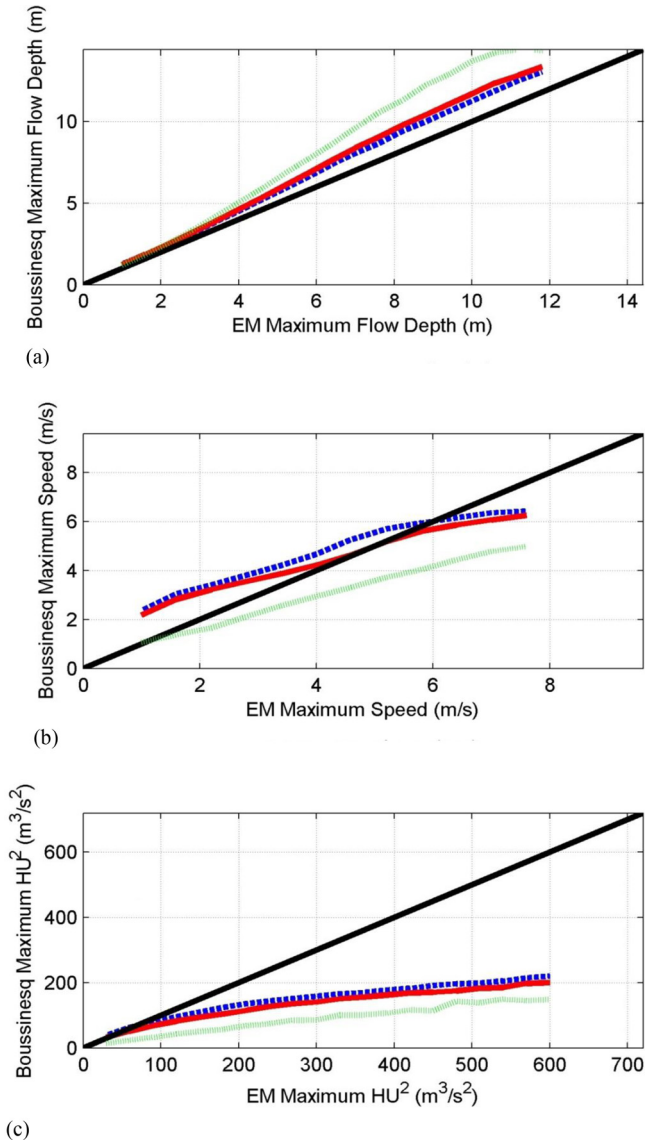

Fig. 5. Comparison of mean regression lines for different initial Froude numbers (F_o = 0.85, bold dashed line; F_o = 1.0, solid line; F_o = 1.4, light dashed line)

coincident. The standard deviation of these values was also found to be quite large as a result of the similarly large variability found in the EM maximum speed predictions.

In the results shown in Figs. 2–4, the EM used an initial Froude number of 1.0. Although this is a physically intuitive value to employ, it is necessary to understand the statistical behavior of the EM with changes in this Froude number. Fig. 5 show the mean regression lines using three different initial Froude numbers: F_o = 0.85, 1.0, and 1.4. Considering the predicted maximum flow depths in Fig. 5(a), it appears that the EM underprediction bias decreased with decreasing F_o, although the difference between values of 0.85 and 1.0 is minimal. The reverse trend was found for the maximum flow speed, shown in Fig. 5(b), with the largest initial Froude number resulting in the greatest EM overprediction bias. The momentum flux, shown in Fig. 5(c), also exhibited this trend, with the highest Froude number tending to predict the greatest momentum flux. All regression lines fell within the area of EM overprediction, with the exception of small momentum flux values when using the smallest initial Froude number. In summary, it is concluded that an initial

J. Waterway, Port, Coastal, Ocean Eng., 2017, 143(5): -1--1

Froude number of 1.0 provides the best balance of accuracy in flow depth and maximum flow speed. In addition, it is always conservative in its prediction of momentum flux, which is a desirable characteristic for the design of critical structures to resist tsunami wave loads.

The results from the Monte Carlo comparisons of the EM and the Boussinesq wave model were found to be somewhat dependent on the range of parameters tested. Sensitivity tests were conducted to evaluate steeper versus milder offshore slopes and onshore slopes. Results showed that varying offshore slope had little effect on the agreement between the Boussinesq modeling and the EM method. For the onshore slope, the correlation trends showed larger differences. By splitting the data set into two groups, half with steeper onshore slopes and half with milder onshore slopes, it was found that flow depths varied by approximately 5% between the two data sets, whereas velocities varied by approximately 20%, and momentum flux varied by about 30%. In general, steeper onshore slopes showed better correlation in flow depth and speed between the Boussinesq and EM.

Evaluation Using *MOST* Simulations for Monterey Bay

As part of the ASCE 7 Tsunami Loads and Effects Committee work, Dr. Yong Wei of the National Oceanic and Atmospheric Administration (NOAA) Pacific Marine Environmental Laboratory (PMEL) performed a simulation of tsunami inundation near Monterey, California, using the NOAA *MOST* tsunami propagation model [e.g., Titov and Synolakis (1997) and Titov and Gonzalez (1997)]. The simulation modeled an M_w-9.5 Alaska earthquake (33.3-m slip over a rupture area of 1,500 km by 100 km) in the Aleutian Islands. A Manning n value of 0.025 was used for both nearshore bathymetry and onshore topography. Results for wave inundation were then saved for an area near Monterey, California. Fig. 6 shows the topographic contours, the maximum water levels, and the inland extent of the tsunami hazard zone from a region of the shoreline just east of the harbor breakwater in Monterey, California. The results were therefore much like a tsunami inundation map that might be published as part of the ASCE 7 standard. In the present case, however, maximum flow depths, flow velocities, and momentum flux were then also saved for numerical grid points on land in this zone. Such detailed information would not be available with a typical inundation map but was used here as ground truth for testing the EM across an array of topographic transects.

Fig. 6 also shows 10 topographic transects that were selected from the inundation map to evaluate the EM. Each transect started at the shoreline and extended past the run-up limit. The *MOST* model results were then obtained approximately every 5 m (16 ft) across transects. Results included the ground elevation, maximum water level or inundation height, maximum flow velocity, and maximum momentum flux. Most transects were selected to match the

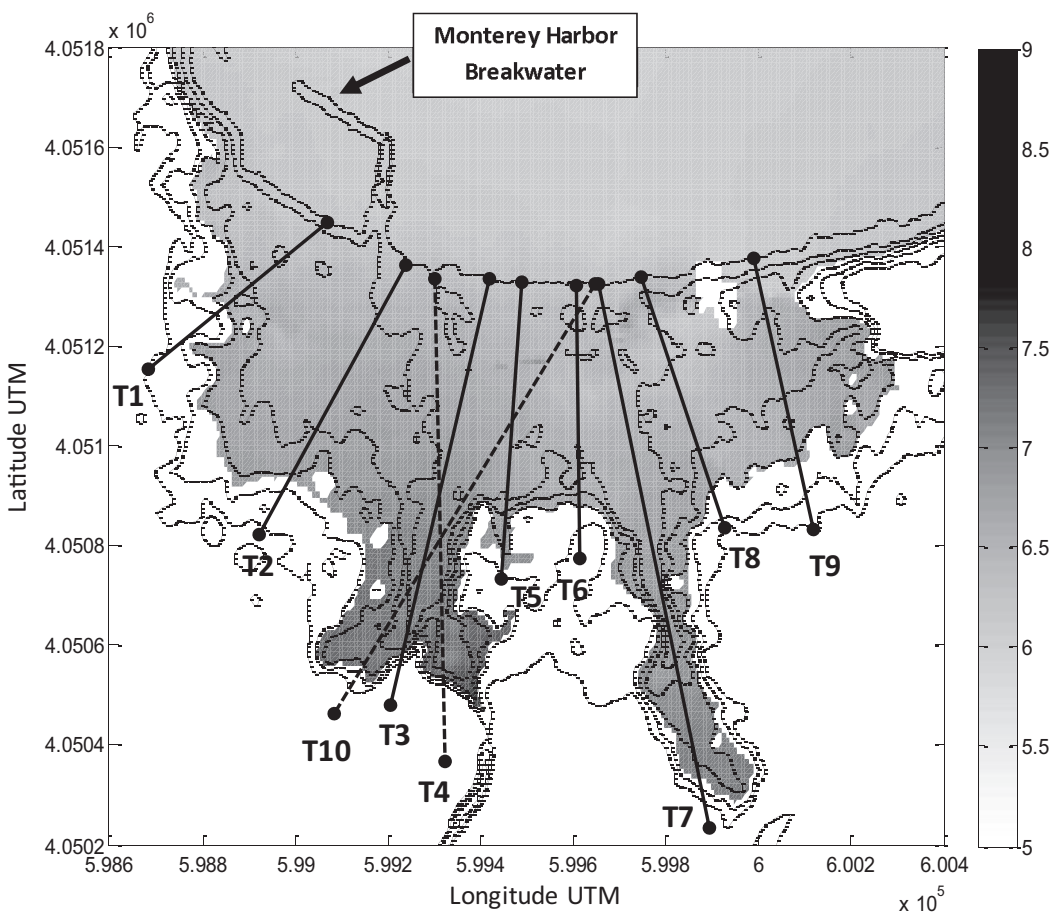

Fig. 6. *MOST* model simulation of tsunami inundation for a region near Monterey, California (Note: Elevation contours of 0, 2, 4, 6, 8, and 10 m shown; shading given for tsunami amplitudes of 5–9 m; lines represent 10 transects simulated using the EM starting at shoreline; dashed transects are purposely nonorthogonal to the shoreline)

J. Waterway, Port, Coastal, Ocean Eng., 2017, 143(5): -1--1

Downloaded from ascelibrary.org by Southern California University on 05/19/17. Copyright ASCE. For personal use only; all rights reserved.

anticipated wave-propagation direction and were roughly perpendicular to the shoreline, but the EM does not rely specifically on any known wave direction, so a few transects were selected at other angles as a test of the method.

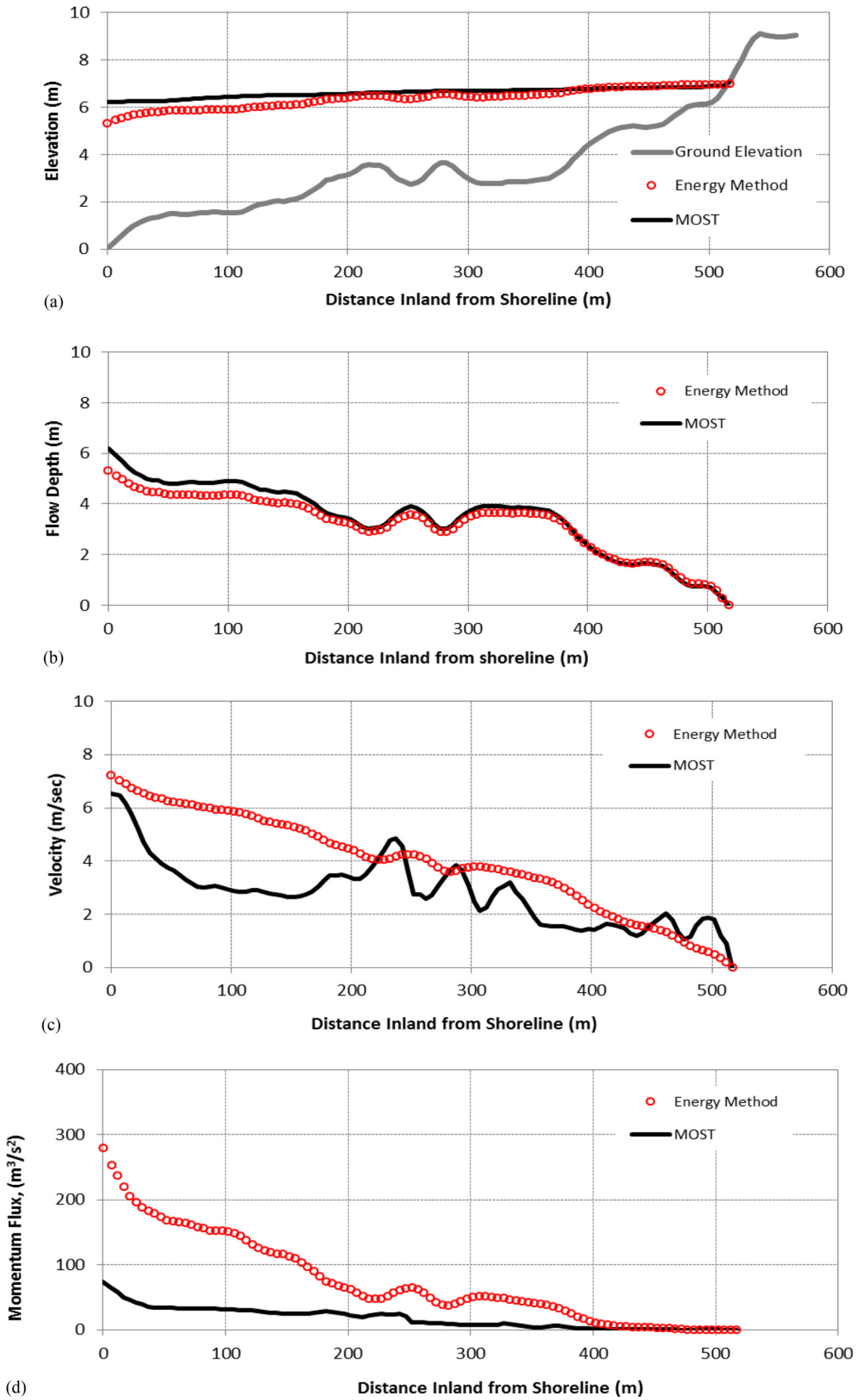

Fig. 7. Comparison of the EM and the *MOST* simulations for Transect T2

J. Waterway, Port, Coastal, Ocean Eng., 2017, 143(5): -1--1

Downloaded from ascelibrary.org by Southern California University on 05/19/17. Copyright ASCE. For personal use only; all rights reserved.

For each transect, the run-up limit from the *MOST* simulation along with ground topography were the only inputs to the EM. The EM was applied using the Froude-number decay from Eq. (12) and with a Manning n value of 0.025, which is generally believed to be suitable for open ground and matches the Manning n value used in the *MOST* simulations. It is noted that neither the *MOST* simulation nor the EM predictions considered actual ground roughness; thus, the Manning n value was kept constant in each model.

Results for selected individual transects are shown in Figs. 7–10. The top panel in each figure shows the ground elevations, along with the maximum water level (inundation height) from the *MOST* simulation (dark solid curve) and the EM (open symbols).

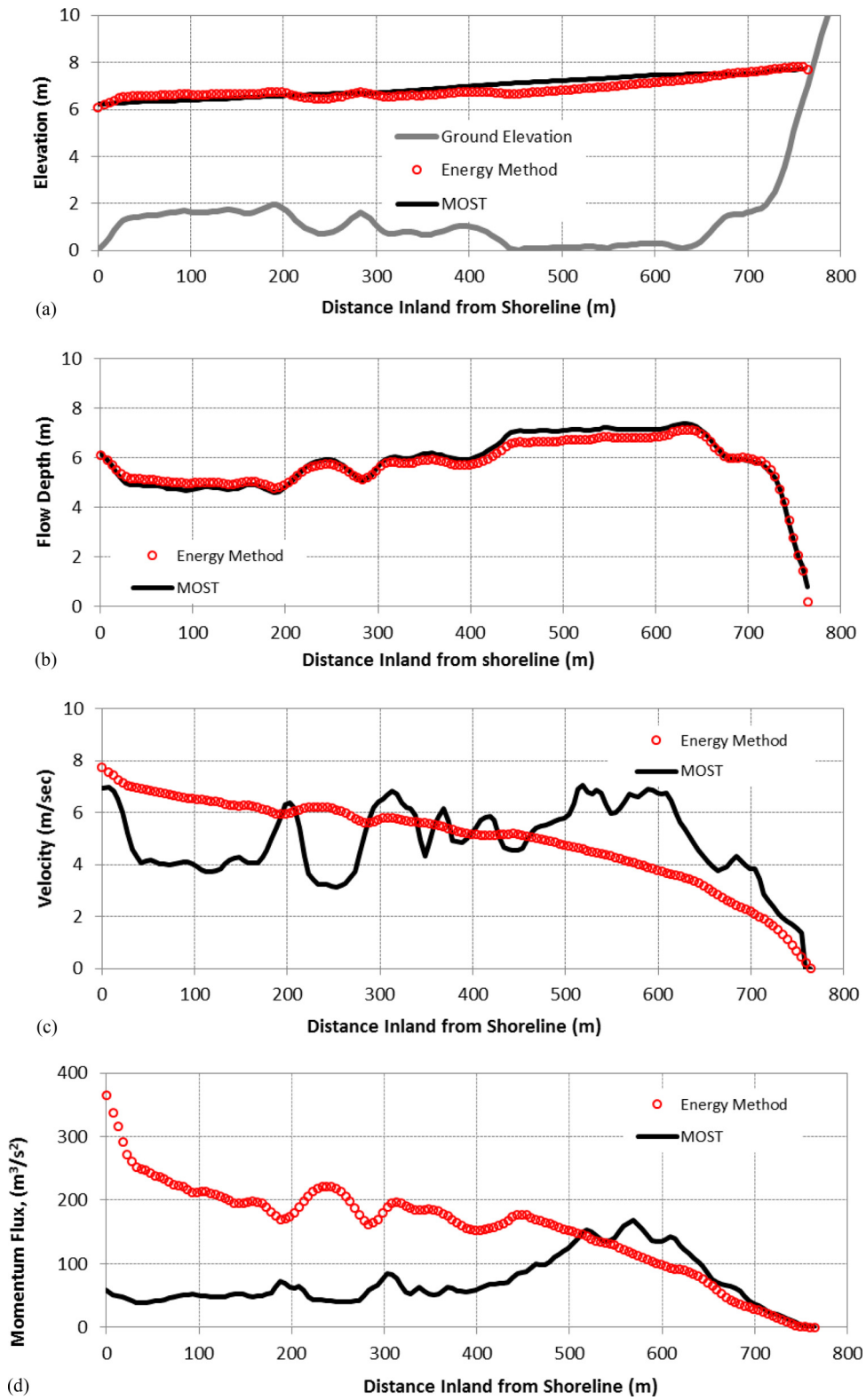

Fig. 8. Comparison of the EM and the *MOST* simulations for Transect T3

J. Waterway, Port, Coastal, Ocean Eng., 2017, 143(5): -1--1

Downloaded from ascelibrary.org by Southern California University on 05/19/17. Copyright ASCE. For personal use only; all rights reserved.

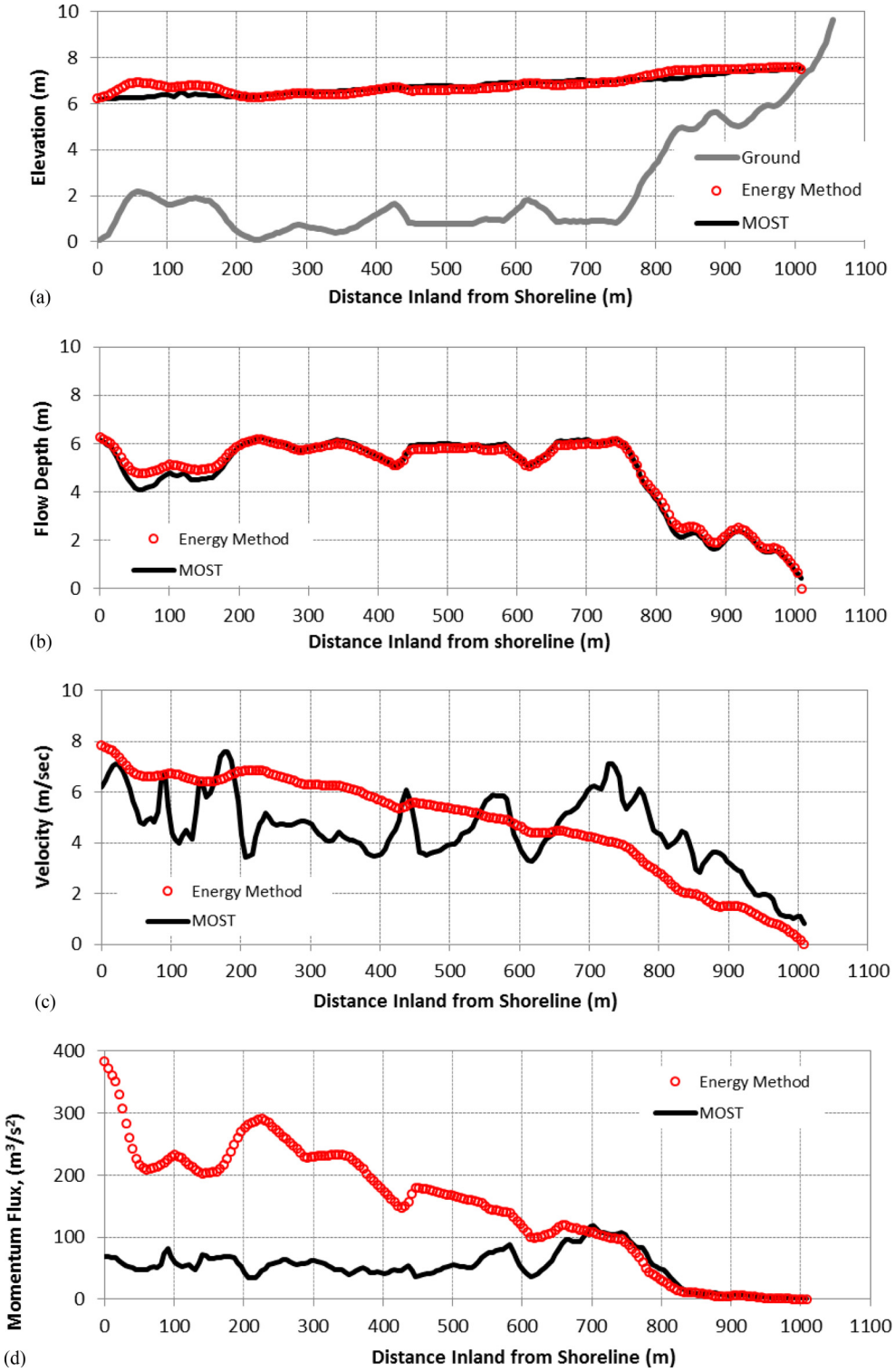

Fig. 9. Comparison of the EM and the *MOST* simulations for Transect T7

The second panel then shows the inundation water depths relative to ground level. The third panel shows the maximum velocity. The fourth panel shows the maximum momentum flux. In the EM, the maximum momentum flux is computed using the product of maximum water level and maximum velocity as $h_{\max}U_{\max}{}^2$. The *MOST* simulations, in contrast, account for time dependence and give the maximum value of instantaneous momentum flux as $(hU^2)_{\max}$.

Figs. 7 and 8 show results for the western portion of the area. Transect T2 (Fig. 7) is relatively short but rises fairly consistently with steep ground slopes, containing just two short regions of negative ground slopes. Transect T3 (Fig. 8) is nearby, but is longer, with lower ground elevations (in fact, with a lake located in a portion), longer sections of negative slopes, and higher tsunami run-up, according to the *MOST* simulation. Figs. 9 and 10 show results for the eastern side of the area. Transect T7 (Fig. 9)

J. Waterway, Port, Coastal, Ocean Eng., 2017, 143(5): -1--1

Downloaded from ascelibrary.org by Southern California University on 05/19/17. Copyright ASCE. For personal use only; all rights reserved.

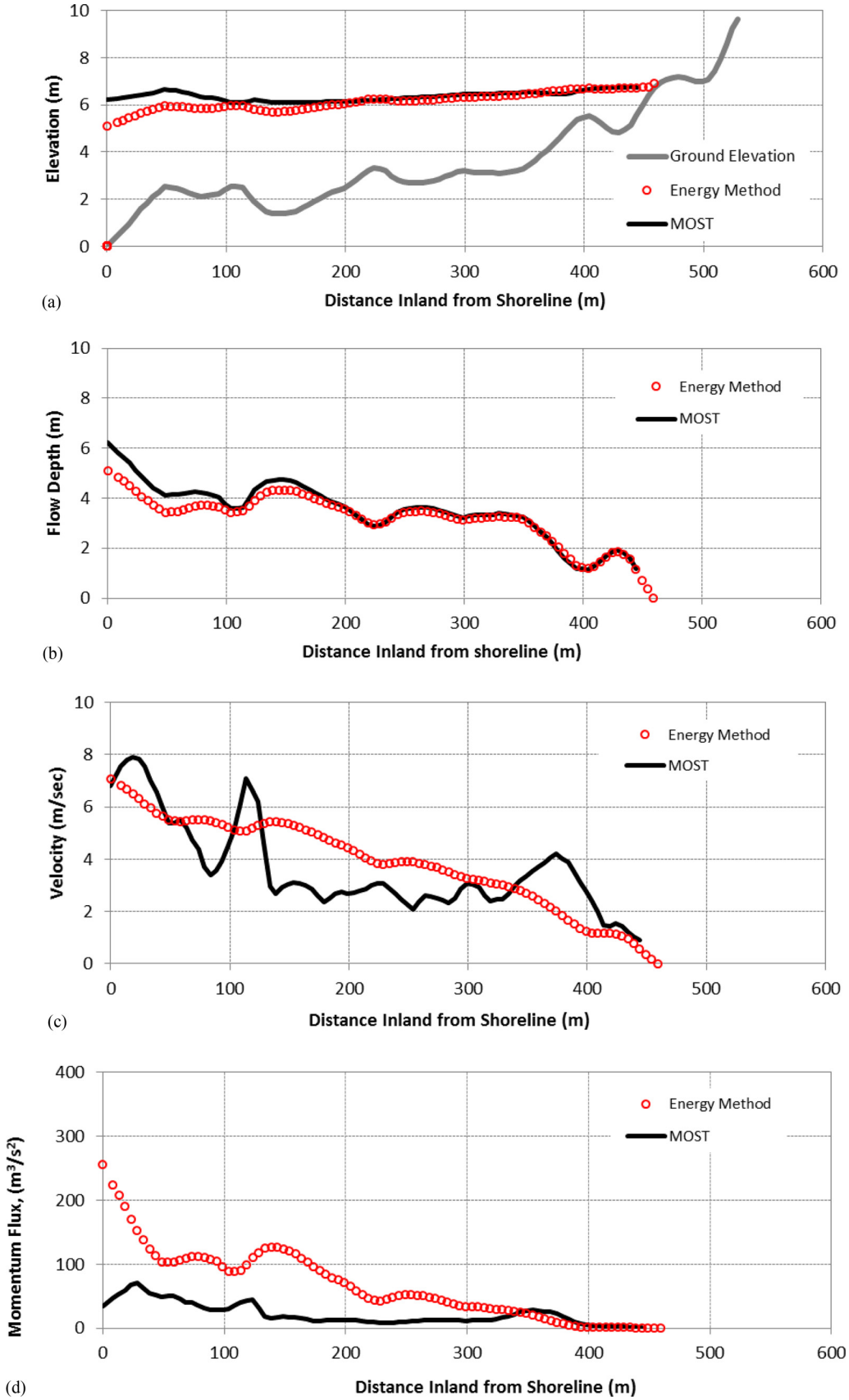

Fig. 10. Comparison of the EM and the *MOST* simulations for Transect T8

follows a narrow valley and is the longest transect simulated (1,040 m), whereas Transect T8 (Fig. 10) is on an adjacent higher bluff, producing a shorter transect over steeper ground with less run-up.

J. Waterway, Port, Coastal, Ocean Eng., 2017, 143(5): -1--1

Downloaded from ascelibrary.org by Southern California University on 05/19/17. Copyright ASCE. For personal use only; all rights reserved.

In all cases, inundation levels were well predicted using the EM. Because the predictions start at a known run-up location, the inundation levels were predicted most accurately near the run-up limit, and errors were largest near the shoreline. Flow depths, however, were predicted quite well across a wide range of ground topographies and ground slopes, including over negative ground slopes. Velocities were predicted reasonably well in the mean sense, in that the EM seemed to simulate the average trajectory or decay of velocities. The *MOST* model included wave run-up and rundown, effects of wave reflection, and lateral convergence and divergence of flows, and it was clearly more sensitive to localized topography, with higher velocities on the landward side of the topographically high features where negative ground slopes occur. Maximum velocities from the *MOST* simulation occurred in both the landward and seaward directions. The EM did not replicate these details and predicted a smoother and more continuous decay of velocity from the shoreline to the run-up limit, with the implicit assumption of maximum velocities in the landward direction. The EM generally overestimated velocities near the coast (with exception for negative ground slopes) but then underestimated velocities closer to the run-up limit, especially for the cases where constriction of a valley would cause horizontal flow convergence that is not included in the EM. Momentum flux was generally overestimated, in some cases considerably, with the most accurate predictions occurring closer to the run-up limit on steeper ground slopes.

Figs. 11–13 show point-to-point comparisons (*MOST* to EM) for each computational point used in the 10 transects. Computational points were spaced approximately 5 m apart, and approximately 1,250 points were included in the comparisons.

Fig. 11 reinforces the observation that inundation levels were well predicted by the EM. In general, there was little systematic bias, and the predictions were tightly clustered about the line of perfect agreement. On average, the *MOST* water levels were just 3% higher than the EM water levels. Maximum errors were approximately plus or minus 20%. A comparison of these results with the *COULWAVE* simulations in Fig. 2 shows that the results for the 10 transects in the *MOST* simulation for Monterey Bay had about the same variability but not as much bias as found earlier.

Fig. 12 indicates that velocity predictions using the EM had little bias but also little precision. The results from the 10 transects in the Monterey Bay simulation show that velocities were predicted well on average but that errors of plus or minus 50% or more occurred. Applications that use the velocity determined from the EM should account for the possibility of large errors in prediction, recognizing that although the general decay of velocities across a transect is predicted reasonably well, there will be localized regions where velocities are above or below the predicted values, as shown in Figs. 7–10.

Fig. 13 shows that the EM overestimated the momentum flux in almost all cases. Similar to what was found in Fig. 4 comparing the EM and the *COULWAVE* model, the EM sometimes underpredicted for small values of momentum flux but systematically overpredicted (often by a factor of 4 or more) for large values of momentum flux. Reasons for the underprediction are not fully known. However, review of Fig. 8 for Transect 3 shows that the underprediction occurred in a valley where very flat ground slopes suddenly transition into very steep ground slopes and where flows (particularly outflows) likely converged. As noted earlier, the EM does not

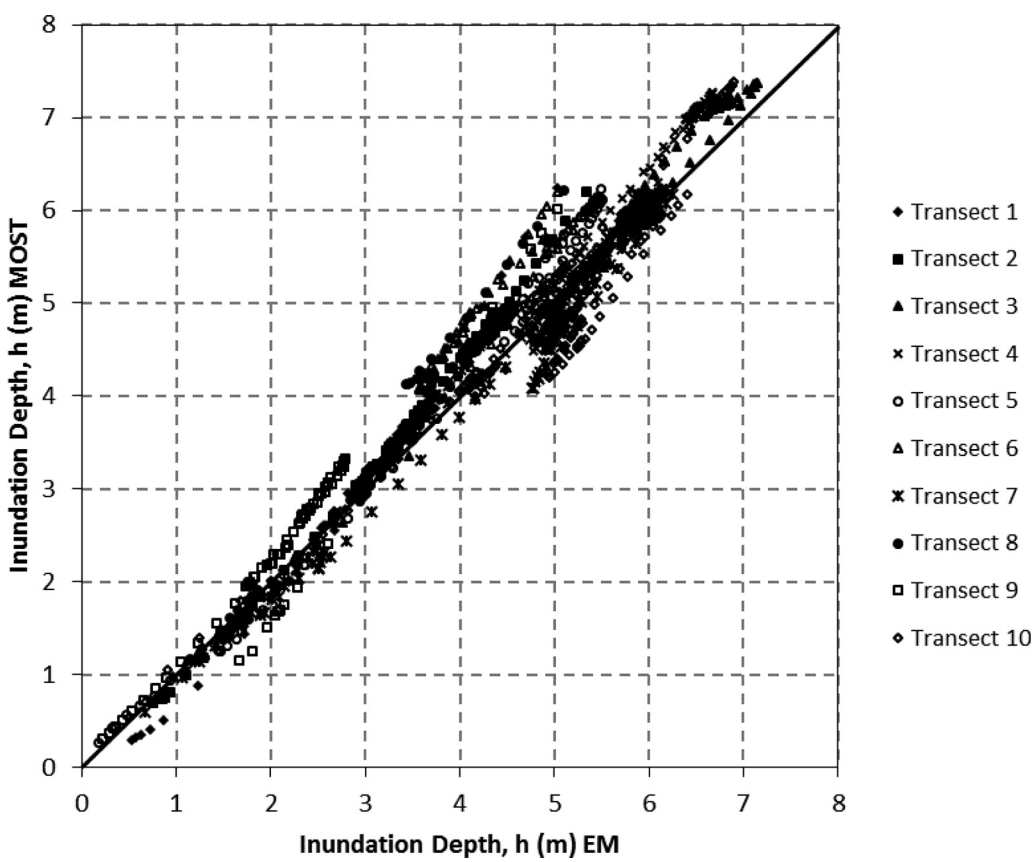

Fig. 11. Comparison of maximum water levels from *MOST* model and EM for 10 transects in the Monterey Bay simulations

J. Waterway, Port, Coastal, Ocean Eng., 2017, 143(5): -1--1

Downloaded from ascelibrary.org by Southern California University on 05/19/17. Copyright ASCE. For personal use only; all rights reserved.

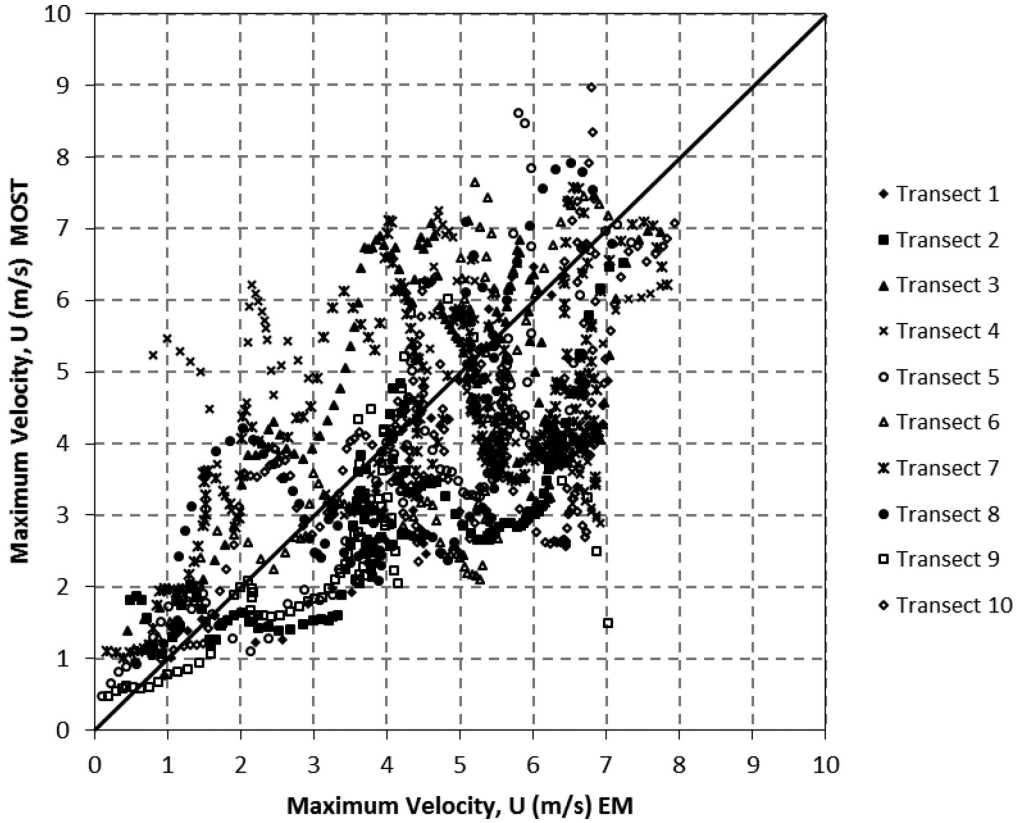

Fig. 12. Comparison of maximum velocities from *MOST* model and EM

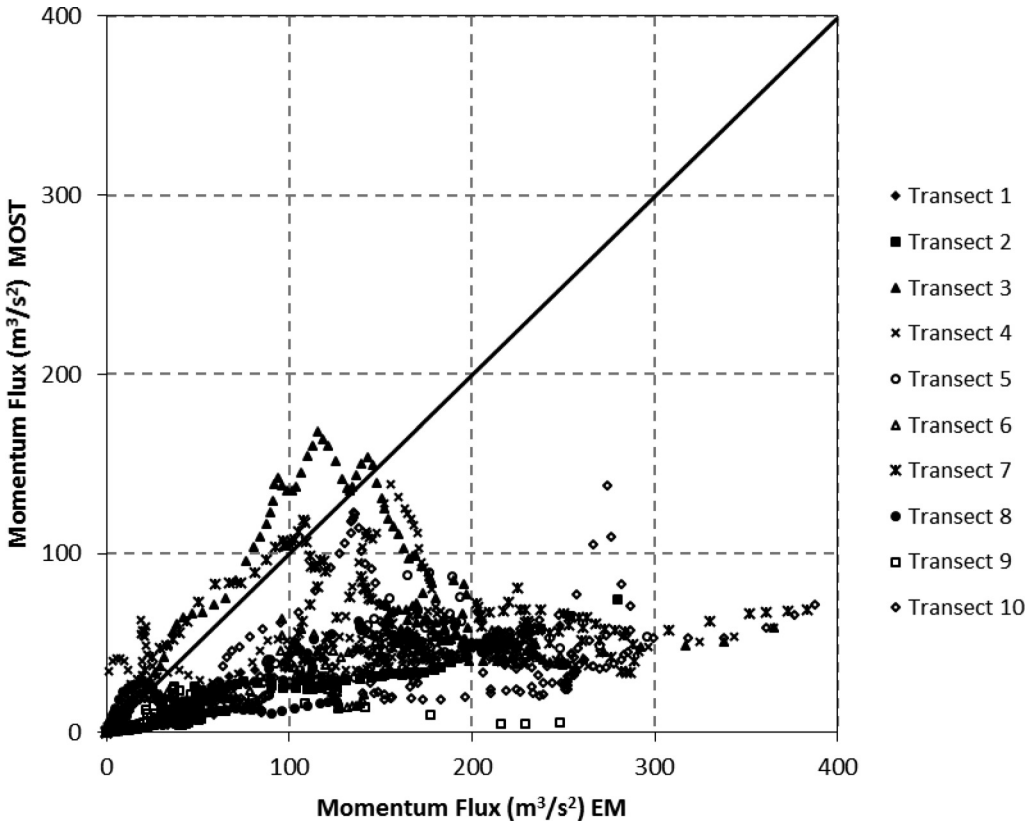

Fig. 13. Comparison of maximum momentum flux from *MOST* model and EM

J. Waterway, Port, Coastal, Ocean Eng., 2017, 143(5): -1--1

Downloaded from ascelibrary.org by Southern California University on 05/19/17. Copyright ASCE. For personal use only; all rights reserved.

account for time dependence, and the results in Fig. 13 show the maximum energy flux computed using the maximum flow depth multiplied by the square of the maximum velocity, whereas the values from the *MOST* simulation show the maximum value of (hU^2) using instantaneous depths and velocities.

The maximum momentum flux in the new ASCE 7 provisions is adjusted to partially account for the phasing between maximum flow depth and maximum flow velocity. Based on other work not done as part of the present study, the new provisions assume that the maximum velocity occurs coincident with a flow depth of about two-thirds of the maximum flow depth. This adjustment is not reflected in Fig. 13 but would essentially reduce the momentum flux values from the EM by a factor of 2/3. As evident from Figs. 4 and 13, the EM will still result in an overestimation of the momentum flux in high-flow conditions, but the degree of overestimation incorporated in ASCE 7 is less than that shown here.

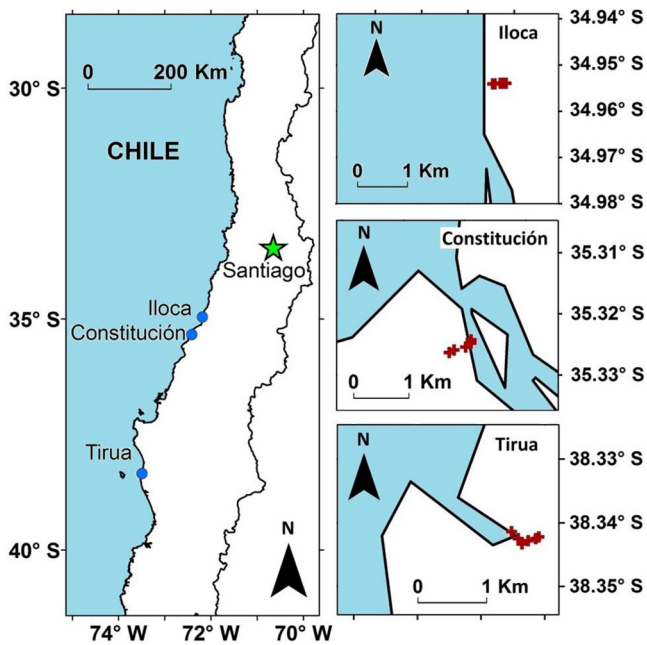

Fig. 14. Water-surface depth profiles surveyed after the M_w-8.8 February 27, 2010, Chile tsunami [Note: Small panels show locations for three transects (crosses)]

Evaluation Using Posttsunami Field Data

Post-tsunami field surveys typically document run-up elevations, inundation depths, and damages immediately after a tsunami event. In certain cases, it is possible to obtain a cross-shore transect of the inundation by surveying marks on vegetation, buildings, and other man-made structures. Elevations obtained for these transects are usually taken to be accurate within a tenth of a meter; however, the accuracy of the elevations is not really known. Such effects as local flow interactions, head loss at structures, and splash-up can lead to marks that are either higher or lower than an undisturbed water surface by several tenths of a meter. Still, these field transects provide an opportunity to examine the effectiveness of the EM predictions.

The EM was compared to several transects of water surface from field surveys for two events, first for the M_w-8.8 February 27, 2010, tsunami in Chile and then for the M_w-9.0 March 11, 2011, tsunami in Japan. Fig. 14 gives the locations of three inundation profiles surveyed at Iloca, Constitucíon, and Tirúa in Chile as part of the 2010 International Tsunami Information Centre/United Nations Educational, Scientific, and Cultural Organization (ITIC/UNESCO) Rapid Reconnaissance Tsunami Survey of March 7–26, 2010 (Fritz et al, 2011; Catalan 2012). The marks were considered quite accurate because they were taken on the flow-parallel face of buildings that lined streets perpendicular to the tsunami inflow. In the cases of Constitucíon and Tirúa, the tsunami propagated from the riverside of the town. Fig. 15 shows survey transects taken at Rikuzentakata in the Iwate prefecture on the Sanriku coast of Japan during March 26–29 and April 9–11, 2011 (Liu et al. 2013). Transects L1 and L2 had quite differing topography: transect L1 was very irregular, whereas L2 was bowl-shaped. Transect L3 was not evaluated because it did not end at a finite run-up point.

For the field transects, the water surface was calculated using the EM, starting with the surveyed run-up elevation and ground elevations taken at major slope breaks. The ground elevations were interpolated between survey points so that the Δx step size did not exceed 9 m (30 ft). Manning roughness was set using engineering judgment of the representative roughness element size with values of 0.03 on the natural coastline, 0.04 in widely spaced urban areas, and 0.06 in closely spaced urban areas. Initial Froude numbers of 1, 1.2, and 1.4 were used to evaluate the dependence of results on the assumption for Froude number.

Figs. 16 and 17 give a comparison of the surveyed transects with EM computations for the two events. In all cases, the water-surface

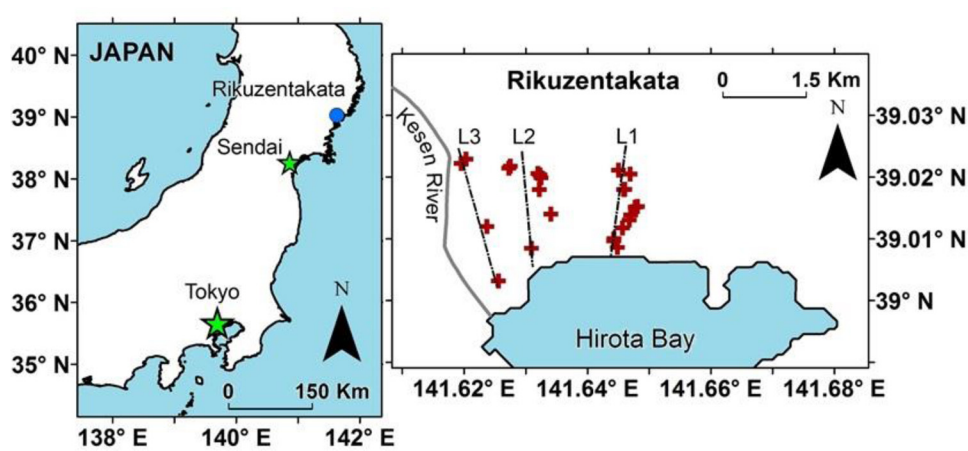

Fig. 15. Water-surface depth profiles surveyed at Rikuzentakata, Japan, after the M_w-9.0 March 11, 2011, Japan tsunami [Note: Transects L1 and L2 are considered with several inundation points indicated by the crosses between the shoreline and run-up limit]

J. Waterway, Port, Coastal, Ocean Eng., 2017, 143(5): -1--1

Downloaded from ascelibrary.org by Southern California University on 05/19/17. Copyright ASCE. For personal use only; all rights reserved.

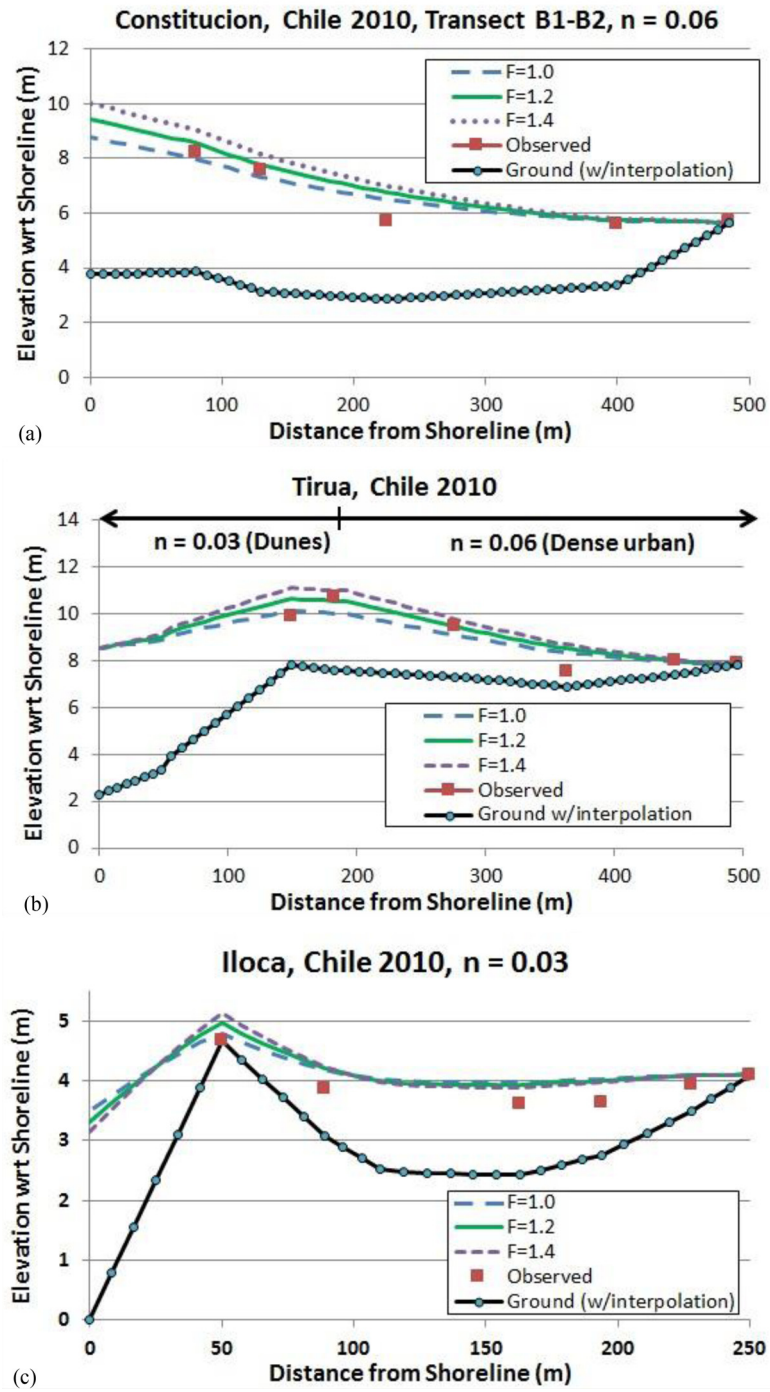

Fig. 16. Comparison between surveyed water surfaces from Chile 2010 tsunami and inundation profiles developed using the EM

profiles predicted by the energy method agreed fairly well with those measured in the field surveys, keeping in mind the intrinsic uncertainty in the forensic observations and the simplicity of the EM. Because the EM does not take into account rapidly varied flow (i.e., subcritical–supercritical flow transitions), for cases where there are large coastal dunes or obstructions, such as shore-parallel road embankments, the inundation predicted by the EM appears to somewhat overpredict the water-surface elevation, especially for short transects.

In the case of Iloca, Chile, shown in Fig. 16, the large coastal dune resulted in local flow acceleration and transition to supercritical flow on the shoreward side followed by a transition back to slower flow speeds. In cases where there are hydraulic jumps associated with overtopping of long lateral structures, the Froude-number behavior assumed for the EM does not strictly hold; however, for purposes of design, this becomes a conservative assumption for both the energy and flow depth at a given location. For long transects, where frictional effects dominate losses resulting from flow transitions, the EM predictions should be more accurate than those for short, hilly transects. It is significant that for Transect L1 at Rikuzentakata, a distance of over 1,700 meters, the prediction at the shoreline using the EM calculated from maximum run-up was very close to what was measured in the field, despite the fact that predictions were less accurate in

J. Waterway, Port, Coastal, Ocean Eng., 2017, 143(5): -1--1

Downloaded from ascelibrary.org by Southern California University on 05/19/17. Copyright ASCE. For personal use only; all rights reserved.

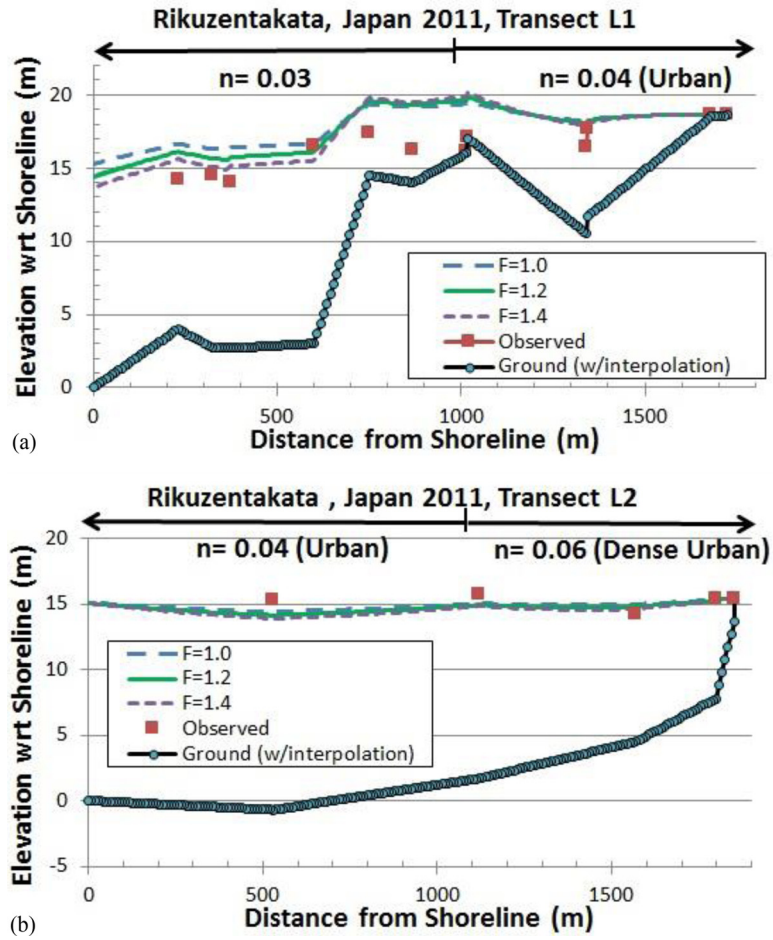

Fig. 17. Comparison between surveyed water surfaces from Japan 2011 tsunami and inundation profiles developed using the EM

between the run-up limit and the shoreline over the topographic high point.

The EM, which was developed for simplified analysis of overland tsunami flows for design purposes, does not account for two-dimensional effects, such as wave convergence, wave reflections, or wave interactions; this is a likely explanation for the slight underestimation of inundation for Rikuzentakata Transect L2. Whereas the other comparisons usually showed the field-observed values below the EM predictions, in this case, the observed values were slightly above the predictions. This area flooded both from the shoreline and from the river, which may account for the locally higher values. Nevertheless, the prediction was still quite close to the field observations.

In general, the EM appears to be a valuable tool to help interpolate and extrapolate sparse field observations. One implication of the beneficial comparison is that run-up elevation measured in the field can be used to estimate inundations between the run-up mark and the shoreline. However, the designer should consider local effects of complex topography and the possibility of wave reflection and interaction. Variation in incident Froude number was found to have relatively little effect. In general, simulations with the EM using an incident Froude number of 1.0 were found to agree more closely with the measured inundation points than simulations with higher incident Froude numbers.

As noted, the results of the EM are based on judgment as to appropriate values of Manning's n based on ground roughness. In particular, the upper limit of $n = 0.06$ was adopted to represent high-density urban areas. Fig. 18 shows selected transects simulated with $n = 0.04$ adopted as the maximum value of Manning's n as might be appropriate for lower-density urban areas. A comparison of results with those in Fig. 16 and 17 shows that when starting at the run-up limit, lower Manning's n values produced lower inundation levels back across the transect to the shoreline, with lower gradients in water levels. Although some data points were better predicted, overall agreement was better in the limited analysis using the higher Manning's n values. Bricker et al. (2015) discussed the selection of Manning's n values and argued that for tsunamis, traditional Manning's n values borrowed from open-channel hydraulic studies are too small. Although the data sample in the current study is too small to be definitive, the results do show that the selection of an appropriate Manning's n can make an important difference when simulating field conditions.

Conclusions

The goal of this study was to apply a simple energy method to predict certain characteristics of overland tsunami flows based on extrapolation of the energy grade line between the shoreline and the tsunami run-up limit. Starting with a mapped run-up or inundation limit from tsunami hazard maps, the method seeks to reconstruct maximum inundation depths and velocities across a flooded topographic transect to the shoreline. The method was developed as a simple and generally conservative method that can be included in a

J. Waterway, Port, Coastal, Ocean Eng., 2017, 143(5): -1--1

Downloaded from ascelibrary.org by Southern California University on 05/19/17. Copyright ASCE. For personal use only; all rights reserved.

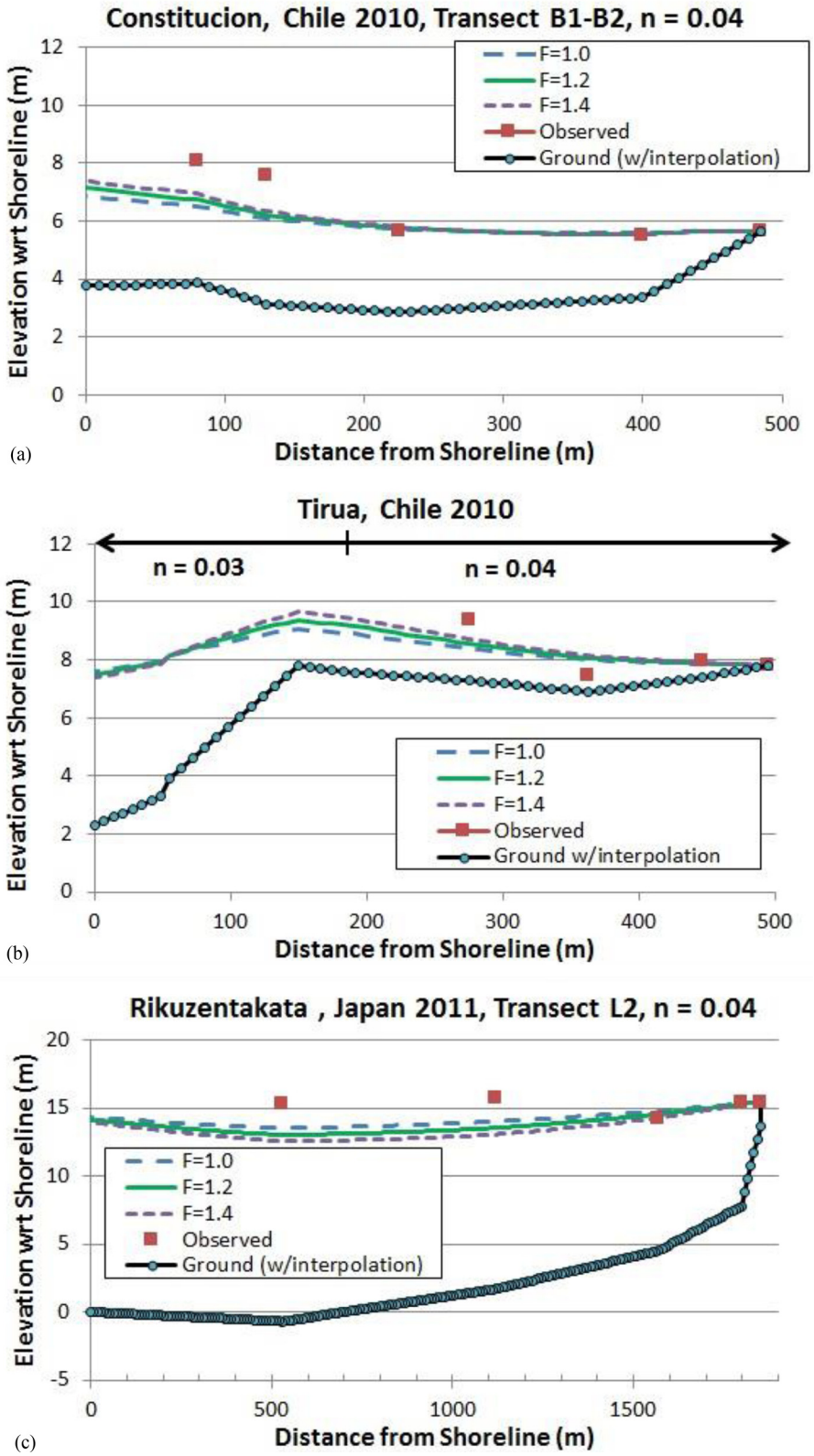

Fig. 18. Selected transects from Chile and Japan using a maximum value of Manning's *n* of 0.04 instead of 0.06, as used in previous examples

new ASCE 7 standard for tsunami loads on buildings. As noted, provisions in the new standard allow end-users to apply more detailed and sophisticated numerical modeling if results of the EM are thought to be too conservative or if the scope of the design warrants more detailed predictions of flow characteristics. But the proposed EM allows a simple first-order estimate of overland tsunami-flow conditions using methods suitable for inclusion in a printed design standard.

Compared with other simplified methods of estimating tsunami-flow conditions, the EM has the advantage of being applicable over

J. Waterway, Port, Coastal, Ocean Eng., 2017, 143(5): -1--1

Downloaded from ascelibrary.org by Southern California University on 05/19/17. Copyright ASCE. For personal use only; all rights reserved.

a wide range of realistic ground topographies, and it allows variable ground roughness across a topographic transect. The method can also be applied using a variety of initial starting conditions. The applications included in this study started at a measured or mapped tsunami run-up or inundation limit, but the method can also be applied using a known tsunami height at the shoreline. The method also can be used to extrapolate inundation levels and run-up elevations measured in posttsunami field surveys because iterative solutions for water levels and velocity can be developed to pass through measured water levels at irregular points across a surveyed transect.

Comparisons of the EM and nonlinear shallow-water wave models indicate that the EM has sufficient accuracy to predict maximum inundation depths, with little bias and good precision across a wide range of flow conditions and topographic conditions. Predicted velocities show little bias but much less precision. Although the maximum velocity decay across a transect can be predicted in a mean sense, the method cannot replicate details of wave reflection, lateral flow convergence, or local flow increase related to supercritical flow past a topographic high point. As a result, local velocities from high-fidelity wave models tend to fluctuate above and below the trend curve predicted by the EM.

The EM generally overestimates the maximum momentum flux, especially in the most damaging high-flow conditions. In some cases, the method can overestimate by a factor of 3 or 4 or more. This is a function of a conservative assumption made here that the maximum inundation depth and maximum velocity occur at the same time. Numerical simulations show that this is not usually the case and that the maximum momentum flux, based on the instantaneous product of point-in-time values of h and U^2, is less than what is predicted using the EM. Although a provision is included in the ASCE 7 standard to compute momentum flux with the maximum velocity but with 2/3 of the maximum flow depth, provisions are still generally conservative to ensure adequate safety and reliability of major structures in tsunami-prone regions.

Acknowledgments

The authors thank Dr. Yong Wei of the PMEL for providing the *MOST* model simulations. Dan Weibe, while a master's degree candidate at Oregon State University, was instrumental in the early evaluation of the method, especially in the evaluation of the Froud-number decay adopted here. This work was performed as part of the ASCE 7 Tsunami Loads and Effects Committee chaired by Mr. Gary Chock. Numerous members of the committee provided useful comments and feedback during the development of this approach.

Notation

The following symbols are used in this paper:

E = specific energy = $h + U^2/2g$;
F = Froude number = $U/(gh)^{1/2}$;
F_o = Froude number at shoreline;
H_L = head loss across transect between shoreline and run-up limit;
h = inundation depth;
h_o = inundation depth at shoreline;
R = mapped tsunami run-up above sea-level reference datum;
S = slope of energy grade line based on Manning equation;
U = overland flow velocity;
U_o = flow velocity at shoreline = $\mathsf{F}_o(gh_o)^{1/2}$;
X = horizontal distance inland from shoreline;
X_R = mapped inundation distance inland from shoreline;
Z = ground elevation above sea-level reference datum; and
ΔX = spatial step for numerical solution.

References

ASCE. (2013). "Minimum design loads for buildings and other structures." ASCE/SEI 7-10, Reston, VA.

Bricker, J. D., Gibson, S., Takagi, H., and Imamura, F. (2015). "On the need for larger manning's roughness coefficients in depth-integrated tsunami inundation models." *Coastal Eng. J.*, 57(2).

Carden, L., Chock, G., Yu, G., and Robertson, I. (2015). "The new ASCE tsunami design standard applied to mitigate Tohoku tsunami building structural failure mechanisms." *Handbook of coastal disaster mitigation for engineers and planners*, M. Esteban, H. Takagi, and T. Shibayama, eds., Elsevier, Amsterdam, Netherlands, 461–490.

Carrier, G. F., Wu, T. T., and Yeh, H. (2003). "Tsunami run-up and drawdown on a plane beach." *J. Fluid Mech.*, 475, 79–99.

Chanson, H. (2006). "Tsunami surges on dry coastal plains: Application of dam break wave equations." *Coastal Eng. J.*, 48(4), 355–370.

COULWAVE [Computer software]. Cornell Univ., Ithaca, NY.

Cox, J. C., and Machemehl, J. (1986). "Overload bore propagation due to an overtopping wave." *J. Waterway, Port, Coastal, Ocean Eng.*, 10.1061/(ASCE)0733-950X(1986)112:1(161), 161–163.

FEMA. (2007). *Guidelines and specifications for flood hazard mapping partners*, Washington, DC.

FEMA. (2012). *Guidelines for design of structures for vertical evacuation from tsunamis*, Washington, DC.

French, J. (1982). "Special computation procedure developed for wave runup analysis for Casco Bay." FIS-Maine, 9700-153, FEMA, Washington, DC.

Fritz, H. M., et al. (2011). "Field survey of the 27 February 2010 Chile tsunami." *Pure Appl. Geophys.*, 168(11), 1989–2010.

Fritz, H. M., et al. (2012). "The 2011 Japan tsunami current velocity measurements from survivor videos at Kesennuma Bay using LiDAR." *Geophysical Res. Lett.*, 39(7).

Fuhrman, D. R., and Madsen, P. A. (2008). "Surf similarity and solitary wave runup." *J. Waterway, Port, Coastal, Ocean Eng.*, 10.1061/(ASCE)0733-950X(2008)134:3(195), 195–198.

Li, Y., and Raichlen, F. (2003). "Energy balance model for breaking solitary wave runup." *J. Waterway, Port, Coastal, Ocean Eng.*, 10.1061/(ASCE)0733-950X(2003)129:2(47), 47–59.

Liu, H., et al. (2013). "The March 2011 Tohoku tsunami survey in Rikuzentakata and comparison with historical events." *Pure Appl. Geophys.*, 170(6), 1033–1046.

Lynett, P. J., Wu, T.-R., and Liu, P. L.-F. (2002). "Modeling wave runup with depth-integrated equations." *Coastal Eng.*, 46(2), 89–107.

Madsen, P. A., and Schäffer, H. A. (2010). "Analytical solutions for tsunami runup on a plane beach; single waves, N-waves and transient waves." *J. Fluid Mech.*, 645, 27–57.

MOST [Computer software]. (2006). Center for Tsunami Research, National Oceanic and Atmospheric Administration, Seattle.

Shen, M. C., and Meyer, R. E. (1963). "Climb of a bore on a beach. Part 3. Run-up." *J. Fluid Mech.*, 16(1), 113–125.

Synolakis, C. E. (1987). "The runup of solitary waves." *J. Fluid Mech.*, 185, 523–545.

Tadepalli, S., and Synolakis, C. E. (1996). "Model for the leading waves of tsunamis." *Phys. Rev. Lett.*, 77(10), 2141–2144.

Taubenböck, H., et al. (2013). "Risk reduction at the "Last-Mile": An attempt to turn science into action by the example of Padang, Indonesia." *Nat. Hazards*, 65(11), 915–945.

Titov, V. V., and Gonzalez, F. I. (1997), "Implementation and testing of the Method of Splitting Tsunami (MOST) model." *NOAA Technical Memorandum ERL PMEL-112*, National Oceanic and

Downloaded from ascelibrary.org by Southern California University on 05/19/17. Copyright ASCE. For personal use only; all rights reserved.

Atmospheric Administration/Pacific Marine Environmental Laboratory, Seattle.
Titov, V. V., and Synolakis, C. E. (1997). "Extreme inundation flows during the Hokkaido-Nansei-Oki tsunami." *Geophys. Res. Lett*, 24(11), 1315–1318.
Weibe, D. M. (2013). "Tsunami inundation: Estimating damage and predicting flow properties." M.S. thesis, Oregon State Univ., Corvallis, OR.
Yeh, H. (2006). "Maximum fluid force in the tsunami runup zone." *J. Waterway, Port, Coastal, Ocean Eng.*, 10.1061/(ASCE)0733-950X(2006)132:6(496), 496–500.

Downloaded from ascelibrary.org by Southern California University on 05/19/17. Copyright ASCE. For personal use only; all rights reserved.